Journal of Magnetism and Magnetic Materials 429 (2017) 1–10

Contents lists available at ScienceDirect

Journal of Magnetism and Magnetic Materials

journal homepage: www.elsevier.com/locate/jmmm

The rheological responds of the superparamagnetic fluid based on Fe_3O_4 hollow nanospheres

Xiaohui Ruan, Lei Pei, Shouhu Xuan, Qifan Yan, Xinglong Gong*

CAS Key Laboratory of Mechanical Behavior of Materials, Department of Modern Mechanics, University of Science and Technology of China, Hefei 230027, PR China

ARTICLE INFO

Keywords:
Magnetic fluid
Fe_3O_4 hollow nanospheres
Stability
Molecule dynamic simulation

ABSTRACT

In this work, a superparamagnetic fluid based on Fe_3O_4 hollow nanospheres was developed and the influence of the particle structure on the rheological properties was investigated. The Fe_3O_4 hollow nanospheres which were prepared by using the hydrothermal method presented the superparamagnetic characteristic, and the magnetic fluid thereof showed well magnetorheological (MR) effect. The stable magnetic fluid had a high yield stress even at low shear rate and its maximal yield stress was dramatically influenced by the measurement gap. In comparison to the Fe_3O_4 nanoparticles based magnetic fluid (MF), the Fe_3O_4 hollow nanospheres based MF exhibited better MR effect and higher stability since the unique hollow nanostructure. The shear stress of the hollow nanospheres is about 1.85 times larger than the nanoparticles based MF because it formed stronger chains structure under applying a magnetic field. To further investigate the enhancing mechanism, a molecule dynamic simulation was conducted to analyze the shear stress and the structure evolution of the Fe_3O_4 hollow nanospheres based MF and the simulation matched well with the experimental results.

1. Introduction

Magnetic fluids, which were composed of magnetic particles in carrier fluids, could change their viscosity in milliseconds in the presence of an external magnetic field (magnetorheological effect). After removing the magnetic field, they return to the starting state. Due to their unique semi-active characteristic, the magnetic fluids have attracted increasing attentions in aviation, apparatus, industrial and biological field, etc.[1–3]. During the past decades, many efforts have been conducted to develop high performance magnetic fluid. Various magnetic particles such as the carbonyl iron (CI), Fe, Ni, Co, Fe-alloy, Fe_3O_4, and ferrite particles were applied in the magnetic fluids [4–6]. Since their high magnetic saturation and tunable sizes, the obtained magnetic fluids presented excellent magnetorheological effect. fabrication, low density, and multiple nanostructures. Due to their unique magnetic property, the Fe_3O_4 based magnetic fluids were widely applied in drug delivery, magnetorheological fluid, MRI imaging, separation and etc.[7,8]. As a matured magnetic material, various methods were developed for tuning the nanostructure of the Fe_3O_4 materials. Various Fe_3O_4 particles such as the nanoparticles [9–12], nanowires [13–15], nanorods [16–18], nanotubes [19,20], nanosheets [21], nanocubes, nanoplatelets, octahedral particles [22–24] and olivary particles [25] have been reported. Although the magnetic saturation of the Fe_3O_4 is smaller than the CI particle, it's compatible surface, small size, and small density match well with the carrying fluid thus presents better stability [26]. To this end, the study of the Fe_3O_4 based magnetic fluid is very important not only for their application but also for fundamental interest [27]. Magnetic particles played the key role in determine the magnetorheological effect for the magnetic fluid [28–30]. Under applying the magnetic field, the magnetic particles assembled to form chain-like structures thus enhanced the viscosity. It was found that the shape of the magnetic particles highly influenced the MR performance. For example, the rod-like particles led to higher MR effect while the wire-like particles improved the stability [31,32]. In comparison to the spherical particles, the anisotropic magnetic particles could result in stronger chains structure due to the larger friction force [33]. The inner structure of the magnetic particles was another critical parameter for the magnetic fluid [34]. Due to its low intensity, the hollow structure would be favorable in magnetic fluid because it could improve the stability [35–38]. Moreover, the chains structure of the hollow particles based magnetic fluid must be very different from the nanoparticles [39]. Therefore, the study of the superparamagnetic fluids based on the Fe_3O_4 hollow nanospheres is valuable.

In this work, a novel magnetic fluid based on the superparamagnetic Fe_3O_4 hollow nanospheres was developed. The hollow structured

* Corresponding author.
E-mail addresses: xuansh@ustc.edu.cn (S. Xuan), gongxl@ustc.edu.cn (X. Gong).

http://dx.doi.org/10.1016/j.jmmm.2017.01.003
Received 12 July 2016; Received in revised form 23 November 2016; Accepted 2 January 2017
Available online 03 January 2017
0304-8853/

Fe_3O_4 nanospheres were synthesized by a simple hydrothermal method and they were further dispersed in the water to form uniform magnetic dispersion. The rheological testing indicated the as-prepared magnetic fluid presented well MR effect with high stability. In comparison to the Fe_3O_4 nanoparticles, the hollow nanospheres based magnetic fluid gave out a better MR performance. A possible enhancing mechanism was proposed to analyze the nanostructure dependent rheological properties in the magnetic fluid. At last, a molecule dynamic simulation was conducted to analyze the magnetic responds of the MF based on hollow particles. These results supplied much valuable information for designing high performance magnetic fluid. Fe_3O_4 was attractive in magnetic fluids because it's easy.

2. Experiment

2.1. Materials

All the chemical reagents were analytical graded and used without further purification. Iron(III) chloride hexahydrate ($FeCl_3{\cdot}6H_2O$; Sinopharm Chemical Reagent Co, Ltd), urea ($CO(NH_2)_2$; Sinopharm Chemical Reagent Co, Ltd), Citric acid trisodium salt dehydrate ($C_6H_5Na_3O_7{\cdot}2H_2O$; Sinopharm Chemical Reagent Co, Ltd), PolyVinylPyrrolidone ($(C_6H_9NO)_n$; Model K-90; Sinopharm Chemical Reagent Co, Ltd), PolyAcrylaMide-3000000 ($(C_3H_5NO)_n$; Sinopharm Chemical Reagent Co, Ltd) and distilled water were used for the synthesis of Fe_3O_4 hollow nanospheres.

2.2. Synthesis of Fe_3O_4 hollow nanospheres

Fe_3O_4 hollow nanospheres were synthesized by a hydrothermal method. Typically, 4 mmol $FeCl_3{\cdot}6H_2O$, 12 mmol $CO(NH_2)_2$ and 8 mmol $C_6H_5Na_3O_7{\cdot}2H_2O$ were dissolved in 40 ml distilled water. After being vigorously stirred to a uniform solution, 0.3 g Polyacrylamide-3000000 and 0.1 g PolyVinylPyrrolidone were added into the solution. Keep stirring until all the reagents were dissolved completely. Then, the mixture was transferred into a 50 ml Teflon-lined autoclave. The autoclave was sealed and then maintained at 200 °C for 12 h. After the autoclave was naturally cooled down to room temperature, the black precipitation was washed with distilled water and absolute ethanol for three times. Finally, the black precipitation was dried in vacuum desiccation oven at 60 °C overnight to get the Fe_3O_4 hollow nanospheres.

For the synthesis of magnetic fluids, the above Fe_3O_4 hollow nanospheres were dispersed into water via sonication. After a uniform suspension was obtained, the final product was sealed in a vial for the further measurement. The magnetic fluids based on Fe_3O_4 hollow nanospheres with weight fraction of 10%, 15%, 20% were prepared. Moreover, in order to compare the difference of the rheological properties in magnetic fluids based on the hollow nanospheres and nanoparticles, the hollow Fe_3O_4 nanospheres was treated under a continuous ball milling for 24 h to achieve the Fe_3O_4 nanoparticles. The Fe_3O_4 nanoparticles based magnetic fluid was prepared after being dispersing in the water. The two magnetic fluids were prepared via a similar process.

2.3. Characterization

The crystal structure of the prepared nanospheres was examined via X-ray diffraction (X-RD) on a Philips X′pert Pro SUPER rotation anode with Cu-Kα radiation (λ=1.541874 Å). A scan rate of 0.02° s^{-1} was applied to record the pattern with the 2θ range of 10–70°. Transmission electron microscopy (TEM) images were obtained on JEOL-2010 with an accelerating voltage of 200 kV. The magnetic property was measured on a superconducting quantum interference device (SQUID) magnetometer at 300 K with the applied field sweeping from −20 to 20 kOe.

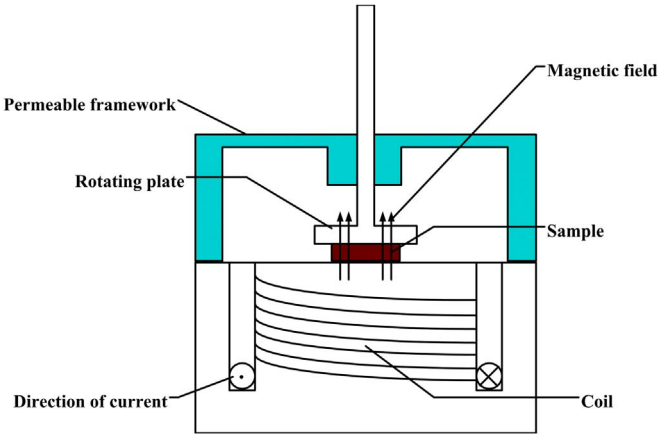

Fig. 1. Principle of testing part for Physica MCR 301.

The rheological properties of the magnetic fluids were tested by a commercial rheometer (Physica MCR 301, Anton Paar Co., Austria). Fig. 1 shows the schematic of the testing part. The samples were placed between two parallel plates and a shear loading was applied on the sample through the rotating plate, which is made of non-permeable material and the diameter of the rotating plate was 20 mm. The rotating plate can also transmit other signals (such as stress, displacement, and strain, etc.) by the sensors connected to it. The magnetic field is generated by an inbuilt coil and the intensity of the magnetic field is controlled by the current in the coil. Magnetic induction lines pass through a permeable framework and sample to form a closed magnetic circuit.

A certain amount of magnetic fluid was taken and put between the two parallel plates of the commercial rheometer. The test was taken out under different shear rate, current and parallel plate gap. All the tests were carried out at room temperature.

3. Result and discussion

3.1. Characterization of the hollow Fe_3O_4 nanospheres

As shown in Fig. 2(a)–(c) are the TEM images of the Fe_3O_4 hollow particles. Clearly, the particles in the images are spherical and the nanospheres had a pale center region and a dark edge, which indicated that the nanospheres had a hollow nanostructure. The average diameter of the magnetite hollow nanospheres was about 300 nm, while the shell thickness was about 40 nm. A higher magnification TEM with one single hollow sphere was used to further investigate the inner nanostructure of the hollow particles. It was clearly observed that the hollow sphere was composed of irregular shaped primary particles with the diameter of approximately 15 nm, which agreed well with the XRD analysis which would be shown later. The shell of the Fe_3O_4 hollow sphere was aggregated by large amount of irregular nanocrystals, thus it was porous. In order to compare the difference of the rheological properties in magnetic fluids based on the hollow nanospheres and nanoparticles, the hollow Fe_3O_4 nanospheres was treated under a continuous ball milling for 24 h to achieve the Fe_3O_4 nanoparticles. Fig. 2(d) showed the TEM image of the final Fe_3O_4 product after the ball milling. Only Fe_3O_4 nanocrystals with size about 15 nm were found. No hollow nanosphere was found in the image, indicated all the particles were broken. This result also supposed that the Fe_3O_4 hollow spheres were aggregated by the secondary Fe_3O_4 nanocrystals.

There are two reasons for the ball milling treatment. Firstly, the ball milling could break the hollow nanospheres into nanoparticles because the nanospheres were composed of large amount of secondary Fe_3O_4 nanocrystals. Secondly, the as-obtained Fe_3O_4 nanocrystals exhibited similar crystal nanostructure and magnetic properties to the Fe_3O_4 hollow spheres, thus they could be used to prepare Fe_3O_4 nanocrystals

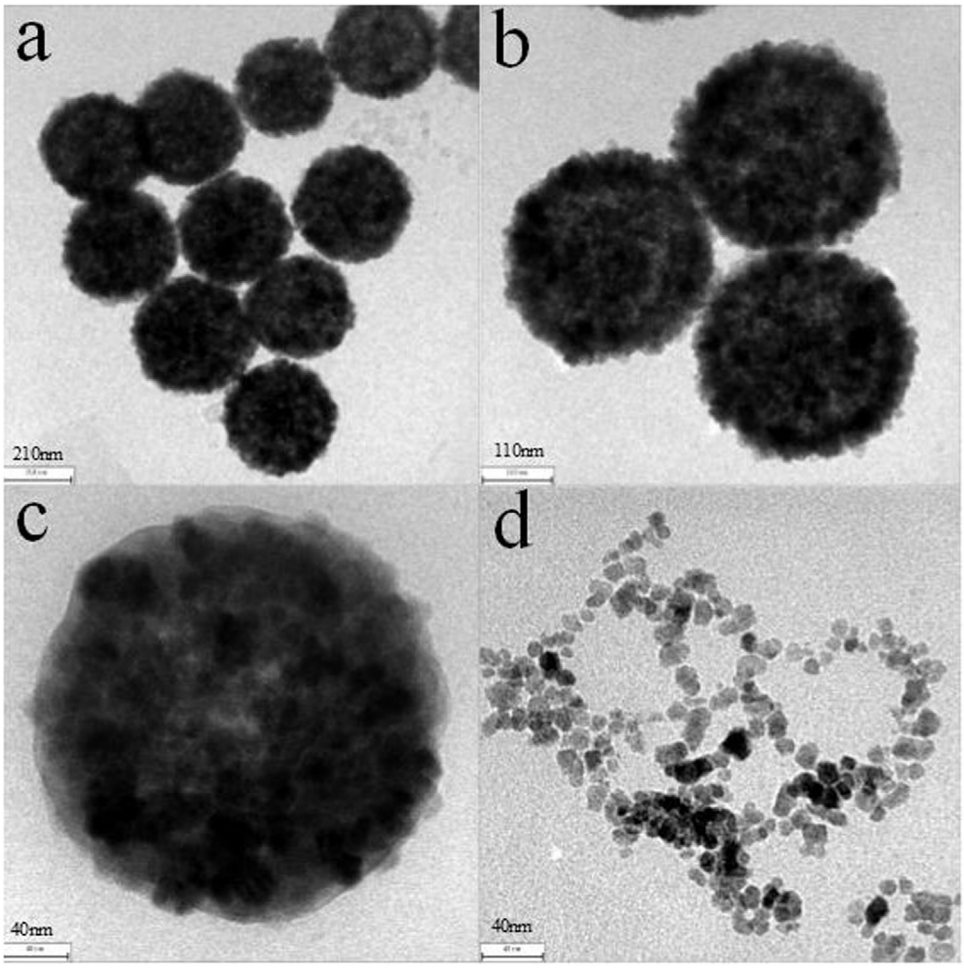

Fig. 2. TEM images of the Fe_3O_4 hollow nanospheres (a), (b), (c) and Fe_3O_4 nanoparticles after ball-milling (d).

based magnetic fluid. The final magnetic fluid was an ideal candidate for analyzing the influence of the nanostructure dependent rheological properties.

Fig. 3(a) shows the XRD pattern for Fe_3O_4 hollow nanospheres. All the sharp peaks in the pattern could be indexed to be the face-centered cubic Fe_3O_4 (JCPDS Card No.75-0033). The broad nature of the diffraction peaks indicates the final product is composed of secondary nanocrystals with average size of 15 nm. No other peak was found in the pattern, indicated the purity of the hollow Fe_3O_4 nanospheres. Here, the obtained Fe_3O_4 nano particles also presented the similar crystal structure to the hollow Fe_3O_4 nanospheres (Fig. 3(b)) although they have different morphologies. Both patterns exhibited the similar

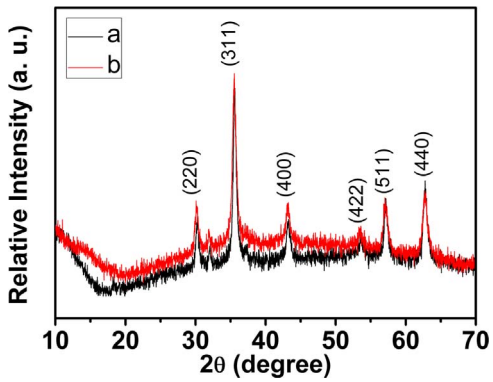

Fig. 3. XRD pattern for Fe_3O_4 hollow nanospheres (a) and Fe_3O_4 nano particles after ball-milling (b).

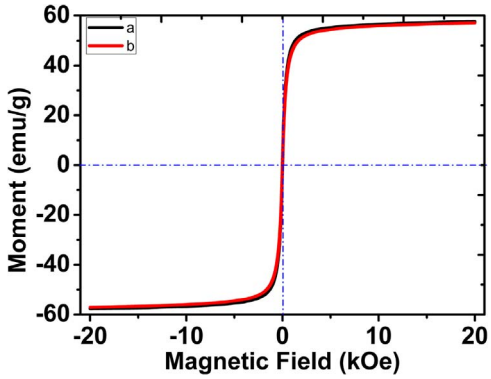

Fig. 4. Hysteresis curves of magnetic Fe_3O_4 hollow nanospheres (a) and Fe_3O_4 nano particles after ball-milling (b) at room temperature.

half-peak-broad, indicated the average grain sizes of the two product were the same.

Fig. 4 showed the field dependence of magnetization for the Fe_3O_4 hollow nanospheres(a) and Fe_3O_4 nano particles after ball-milling(b). The curves exhibited the typical superparamagnetic characteristic and the remnant magnetism was nearly zero. The saturated magnetization (M_S) of the Fe_3O_4 hollow nanospheres was 57.65 emu/g. Although the M_S is smaller than the bulk Fe_3O_4 particles, the value is similar to most of the previous reported Fe_3O_4 particles used in the magnetic fluid. Therefore, this kind of Fe_3O_4 hollow nanospheres is suitable for magnetorheological fluid. More importantly, the hollow nanospheres was composed of secondary Fe_3O_4 nanocrystals with size smaller than

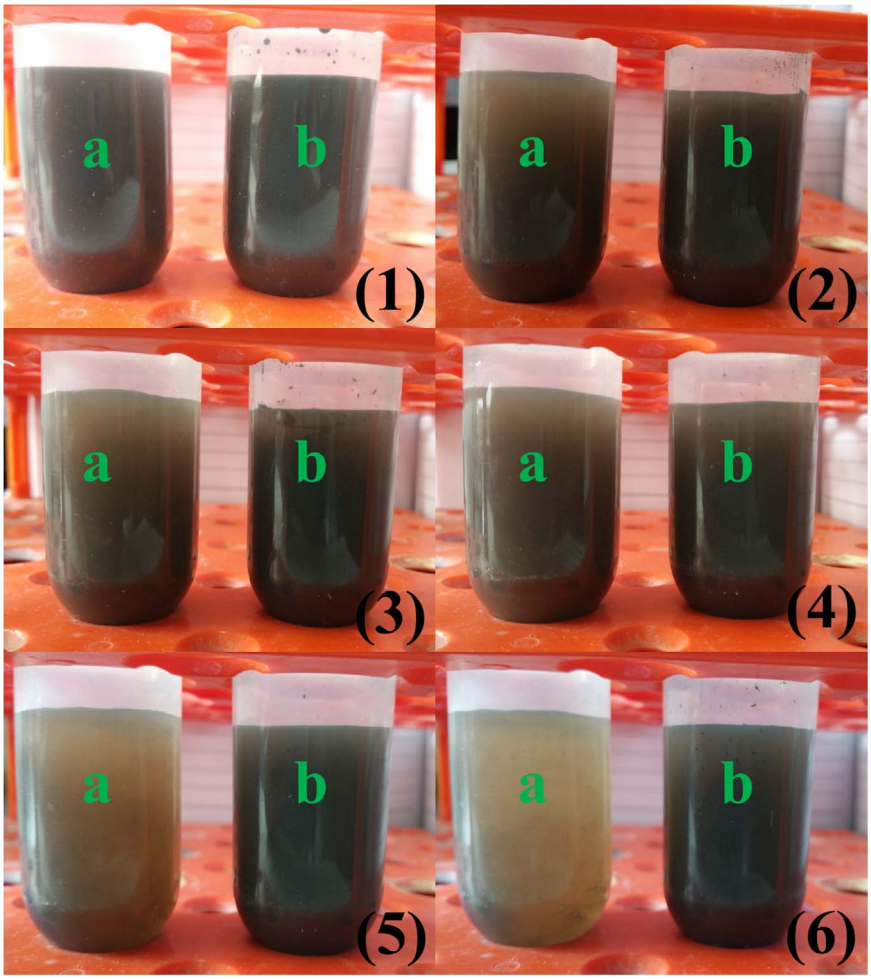

Fig. 5. Stability experiment results for Fe_3O_4 nano particles (a) and Fe_3O_4 hollow nanospheres (b).

30 nm, thus the as-prepared particles were superparamagnetic. The magnetic fluid prepared by the superparamagnetic Fe_3O_4 hollow nanospheres would be more stable than the ferromagnetic fluid. Most importantly, the Fe_3O_4 nanoparticles presented the same magnetic propertied to the Fe_3O_4 hollow nanospheres. In consideration of the similar property, these two particles were the ideal candidate for investigating how does the hollow structure influence the mechanical properties.

3.2. Stability of the magnetic fluids based on the Fe_3O_4 hollow nanospheres

An experiment has been taken out to compare the stability properties of the magnetic fluids based on Fe_3O_4 hollow nanospheres and Fe_3O_4 nanoparticles. The weight fraction of the two kinds of magnetic fluids used for the stability testing was 20% and a centrifugal machine was used. Firstly, 40 ml magnetic fluid based on hollow nanospheres and 40 ml magnetic fluid based on nanoparticles were put into two centrifuge tubes, respectively. The centrifugal speed was 2000 r/min. The states of the two kinds of magnetic fluids were recorded by a camera after centrifuging for 10 min (Fig. 5), then the tubes were put into the centrifugal machine carefully and centrifuging for another 10 min. This process was repeated until the two kinds of magnetic fluids did not appear obvious change.

These two kinds of magnetic fluids were dealt with an ultrasonic machine and the state is shown in Fig. 5(1). It can be found that these two kinds of magnetic fluids were both dispersed uniformly. Fig. 5(2) was got after centrifuged for 10 min and the sedimentation was taken place for the magnetic fluid based on Fe_3O_4 nanoparticles. Fig. 5(3)–(6) were the experiment results of centrifuging for 20, 30, 40, 50 min, respectively. After centrifuging for 50 min, the sedimentation of the magnetic fluid based on Fe_3O_4 nanoparticles was very serious and the sedimentation of the magnetic fluid based on Fe_3O_4 hollow nanospheres was very slight. Based on the above result, it was found that the stability property of the magnetic fluid based on Fe_3O_4 hollow nanospheres was more excellent than the magnetic fluid based in Fe_3O_4 nanoparticles.

3.3. Rheological properties of the magnetic fluid based on the Fe_3O_4 hollow nanospheres

To study the rheological properties of the magnetic fluid based on the hollow Fe_3O_4 nanospheres, three kinds of magnetic fluids with weight fraction of 10%, 15%, 20%, respectively, were prepared. Each kind of suspension was tested under different shear rate, magnetic flux density and gap between the parallel-plates of the rheometer.

Firstly, the shear rate dependent shear stress of the magnetic fluid was studied. Here, the test was taken out on a commercial rheometer with shear rate sweeping logarithmically from 0.01/s to 100/s. Fig. 6 showed the influence of the magnetic flux density and different gap on rheological properties of the 10 wt% magnetic fluids. It can be seen that the shear stress vs. shear rate curves can be divided into two phases. In the first phase, the shear stress increased immediately when the shear rate was applied and in the second phase it increased slowly or kept at a constant. When shear was applied in the presence of an external magnetic field, the magnetic particles would aggregate to form chain-

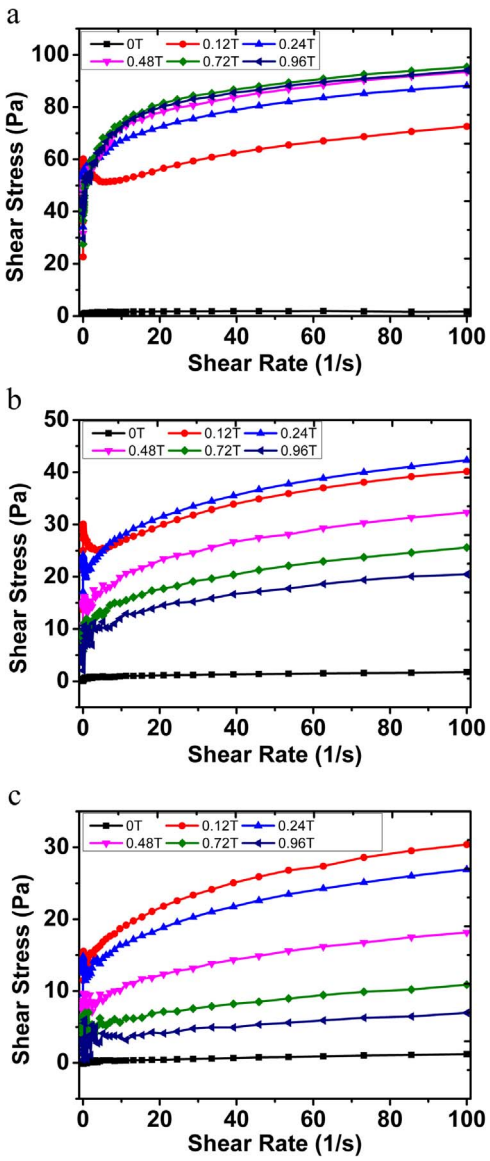

Fig. 6. The transformations of the shear stress with the change of the shear rate under for the 10 wt% magnetic fluid under different magnetic flux density and the gap was 0.6 mm (a), 0.8 mm (b) and 1.0 mm (c), respectively.

like structures parallel to the direction of the external magnetic field to resist the shear, so a yield stress appeared. This typical phenomenon can be described by Bingham model:

$$\begin{aligned} \tau &= \tau_0 + \eta(\dot{\gamma})\cdot\dot{\gamma} \quad |\tau| \geq \tau_0 \\ \dot{\gamma} &= 0 \qquad\qquad\quad |\tau| < \tau_0 \end{aligned} \tag{1}$$

τ_0 was the yield stress of the magnetic fluid based on Fe_3O_4 hollow particles. When the shear stress τ was smaller than the yield stress τ_0, the suspension was in a solid-like state. Then, the shear stress decreased after being yielded and this phenomenon was originated from the slippage between the particle-links and walls. When the shear stress τ was larger than the yield stress τ_0, the magnetic fluid would transform back to a fluid-like state. Here, $\eta(\dot{\gamma})$ was the viscosity of the suspension, it decreased with the increasing of the shear rate.

The curves in the Fig. 6 were fit by formula (1) and then τ_0 and $\eta(\dot{\gamma})$ were obtained (Table 1). It could be seen from Table 1 that a yield stress existed in the curves when an external magnetic was applied. Clearly, the changing of the yield stress τ_0 under different magnetic flux density was complex. With increasing of the magnetic field, the yield stress τ_0 and $\eta(\dot{\gamma})$ would first increase and then decrease. While the external magnetic field is 0.12 T, both of them reached the maximum value.

Table 1
τ_0 and $\eta(\dot{\gamma})$ under different conditions for the gap was 1 mm.

Flux Density	0 T	0.12 T	0.24 T	0.48 T	0.72 T	0.96 T
τ_0 (Pa)	0.08981	14.93311	13.45178	8.16997	4.96299	2.86519
$\eta(\dot{\gamma})$ (Pa·S)	0.01312	0.19863	0.1676	0.12488	0.06882	0.0479

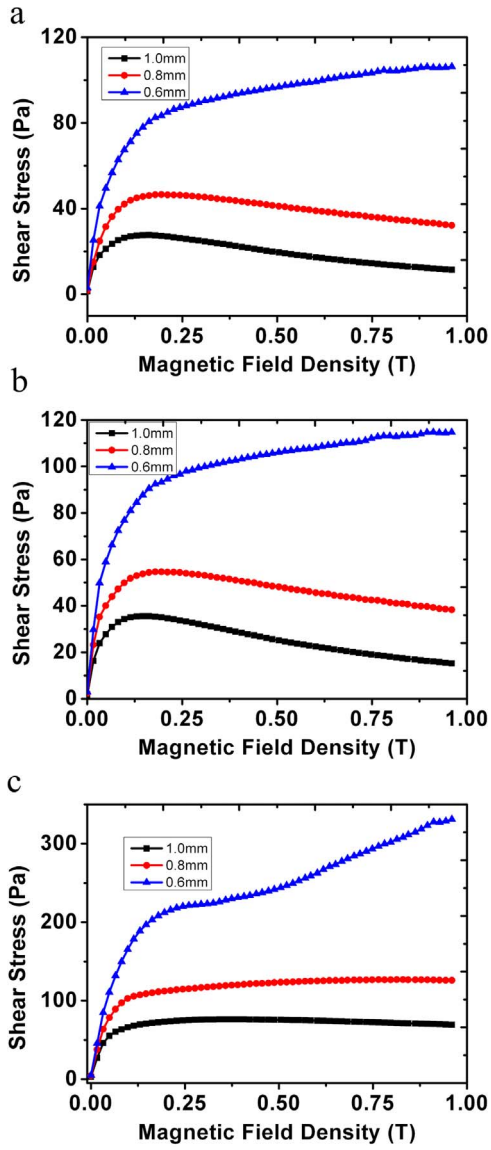

Fig. 7. The transformations of the shear stress with magnetic flux density under different gap of the parallel-plate for different weight percent, (a) for 10 wt%, (b) for 15 wt%, (c) for 20 wt%.

The transformation of the magnetic fluid between solid-like and fluid-like states happened in millisecond order and was reversible. The curves of the shear stress vs. shear rate for the 15 wt% and 20 wt% magnetic fluids were similar with that of the 10 wt% magnetic fluid, so they were not shown here for brevity.

Secondly, the magnetic flux density dependent shear stress of the magnetic fluid was studied. The tests were taken out on the commercial rheometer with magnetic flux density sweeping from 0 T to 0.96 T linearly. The shear stress changing along with the magnetic flux density under different gap was shown in Fig. 7. It could be observed that the shear stress firstly increased along with the external magnetic field and

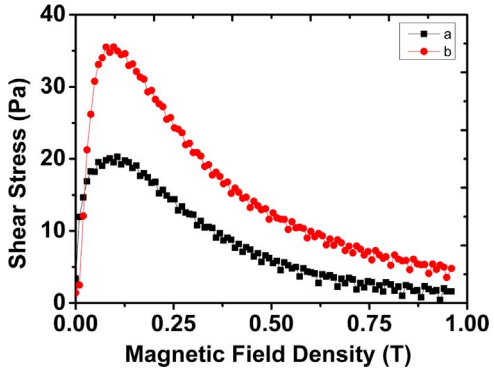

Fig. 8. The rheological properties for Fe_3O_4 nanoparticles (a) and Fe_3O_4 hollow nanospheres (b).

then decreased when the gap was 1 mm and 0.8 mm for the 10 wt% and 15 wt% magnetic fluids. But for the 20 wt% magnetic fluid (Fig. 7(c)), the shear stress increased with the increasing of the external magnetic field no matter how large the gap was. The reason for this will be expounded later on.

In this work, to investigate the influence of the hollow structure on the rheological properties of the magnetic field, both the fluids based on the Fe_3O_4 hollow nanospheres and Fe_3O_4 nanoparticles were tested. Typically, the two magnetic fluids exhibited the magnetorheological effect. In comparison to the nanoparticles, the yield shear stress of the hollow Fe_3O_4 nanospheres is higher (Fig. 8), which further indicated the rheological property of the hollow spheres is more excellent. Because the crystallization and the magnetic properties of the two particles were similar, the enhanced MR effect must be responded to the hollow nanostructure.

The reason for the above phenomenon will be explained. From the TEM images, we can get that the diameter of the hollow nanospheres is about 300 nm and the diameter of the nano particles after ball-milling is about 15 nm. So, we can work out that one hollow particle is composed by about 1600 secondary nanoparticles. We assume that the interaction force only exists between the neighboring particles and the particles arrange along the direction of the external magnetic field. Under the assumption of dipole model, the interaction force between two neighboring particles can be express as:

$$F = \frac{3\mu_0}{2\pi r^4 \mu_1} m \cdot m. \tag{2}$$

So, we can get the interaction force of the hollow particles (Fig. 8(a)) and the nanoparticles (Fig. 8(b)):

$$\mathrm{F}_a = \frac{3\mu_0}{2\pi (2R)^4 \mu_1} nm \cdot nm \tag{3.1}$$

$$\mathrm{F}_b = \frac{3\mu_0}{2\pi (2r)^4 \mu_1} m \cdot m \tag{3.2}$$

and n=1600.

We can also get from Fig. 9 that the contact area of hollow particles is about 9–16 times of that of the nanoparticles. So, we can finally get that the stress of the hollow nanospheres is about 1.25–2.22 times of that of the nanoparticles under the same external magnetic field. Another reason for this is that hollow nanospheres can assemble more chains than the nanoparticles under the condition of the same weight fraction because of the hollow structure. While the particles are bearing a shear, the contact area and the direction of the particles chains will be changed. That would lead the changing of the ratio of the stress. So, the ratio of the stress of these two kinds of particles would be changing continually and this fits well with the experimental results shown in Fig. 8.

The weight fraction of the magnetic fluid and testing gap critically

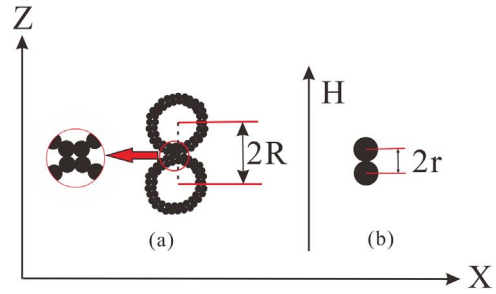

Fig. 9. The interaction schematic for Fe_3O_4 hollow nanospheres and Fe_3O_4 nanoparticles.

affected the measuring results. Fig. 9 were the schematic diagram of the process for Fe_3O_4 hollow nanospheres and Fe_3O_4 nanoparticles changing from a random structure to a chain-like structure when an external magnetic field. This process was depended on the acting force between the particles when the external magnetic field was applied. So, firstly the acting force between the particles was analyzed. The acting force between particles was primarily composed by four parts:

$$\overrightarrow{F} = \overrightarrow{F}_{ij}^{m} + \overrightarrow{F}^{fr} + \overrightarrow{F}_{ij}^{r} + \overrightarrow{F}_{ij}^{v} \tag{4}$$

where $\overrightarrow{F}_{\mathrm{ij}}^{m}$ was acting force between the magnetic dipoles, $\overrightarrow{F}^{fr}$ was friction force, $\overrightarrow{F}_{ij}^{r}$ was repulsive force between the particles and $\overrightarrow{F}_{ij}^{v}$ was Van der Waals (VDW) force. The movement of the particles is slightly influenced by the repulsive force and VDW force, so they could be ignored in this work.

The acting force between the magnetic dipoles $\overrightarrow{F}_{\mathrm{ij}}^{m}$ could be calculated by the formula [40]:

$$\overrightarrow{F}_{ij}^{m} = F_0 \left(\frac{\sigma}{r_{ij}}\right)^4 [(3\cos^2\theta_{ij} - 1)\overrightarrow{r} + \sin(2\theta_{ij})\overrightarrow{\theta}] \tag{5.1}$$

$$F_0 = \frac{3}{16}\pi\mu_0\mu_f\sigma^2\beta^2 H_0^2, \ \beta = \frac{\alpha - 1}{\alpha + 2}, \ \alpha = \mu_p/\mu_c \tag{5.2}$$

where $\overrightarrow{r}$, $\overrightarrow{\theta}$ and $\overrightarrow{z}$ were the unit vectors for the spherical coordinates, H_O was the external magnetic flux density, μ_0 was the permeability of vacuum.

The friction force was composed by two parts, one was the friction force between particles and wall, the other was the friction force between particles and particles.

$$\overrightarrow{F}_i^{fr} = \mu_i \overrightarrow{N_i} \tag{6}$$

$$\overrightarrow{F}_{ij}^{fr} = \mu_{ij} \overrightarrow{F}_{ij}^{r} \tag{7}$$

where $\overrightarrow{F}_i^{fr}$, μ_i, $\overrightarrow{N_i}$ were the friction force, friction coefficient and normal force between particles and wall, respectively; $\overrightarrow{F}_{ij}^{fr}$, μ_{ij} were the friction force, friction coefficient between the particle and particle, respectively. $\overrightarrow{F}_{ij}^{r}$ is small in comparison with $\overrightarrow{N_i}$, so $\overrightarrow{F}_{ij}^{r}$ could be ignored in our research. The friction force between particles and wall was determined by the normal force caused by the shear [41] and the friction coefficient.

When an external magnetic field was applied, particles assembled to form chain structure along the direction of the external magnetic field. In this case, a normal force suddenly appeared between the particles and wall. With the increasing of the shear rate, the chains' tilt angle became larger, which caused the interaction force between the particles transforming from repulsion to attraction [42]. The further increment of the shear rate led to rupture of the chains, thus the normal force disappeared. So, the friction force between particles and wall would decrease or disappear while the shear was applied. Under the influence of the external magnetic field and shear, the chains would rupture and regroup ceaselessly until reached a dynamic equilibrium

state. Similarly, the aggregations of particles changed from a chain-like structure to a cluster-like structure which would decrease the number of aggregations. The touch between the aggregations and wall would also decrease and this would lead to a decrease of the friction force. So the friction force suddenly increased under the applied magnetic field and then decreased with the increasing of the shear rate and the external magnetic field.

The acting force between the magnetic dipoles increased with the increasing of the external magnetic field. After the magnetization intensity of particles was saturated, the acting force between the magnetic dipoles would no longer increasing with the increasing external magnetic field. So the shear stress increased rapidly when the external magnetic field was applied, and then increased gently after the magnetization of the particles reaching saturation.

When the gap between the parallel-plate of the rheometer was changed, the trend of the shear stress according to the shear rate changed. This was because that the gap between the parallel-plate of the rheometer would have an obviously effect on the normal force. The normal force could be expressed as follow [41]:

$$\overrightarrow{N} = \frac{2\tau_0 V^{3/2}}{3\pi^{1/2}h^{5/2}}\vec{n}_0 \tag{8}$$

where V was total volume of the magnetic fluid, τ_0 was the yield stress of the magnetic fluid and h was the gap distance of the rheometer. It could be seen that the normal force would increase rapidly when the gap distance was decrease, so the friction would increase.

The acting force between the magnetic dipoles and the friction force would increase when the external magnetic field was applied and then decrease along with the increasing of shear rate. The friction force would increase along with the decreasing of the gap distance and decrease along with the increasing of shear rate. Therefore, the shear stress would increase rapidly while an external magnetic field was applied and then decrease while the shear rate was increasing with a larger gap distance. For the smaller gap distance, the shear stress would be mainly determined by the friction force (Fig. 10).

3.4. Molecular dynamic simulation of the magnetic fluid based on the Fe3O4 hollow nanospheres

The acting force between the Fe3O4 hollow nanospheres was studied. Liu et al.[43] has proposed an easy-to-use modified dipolar force model $\vec{\mathbf{F}}_{ij}^{\,m}$, which is preferred to describe the magnetic interaction force of two close magnetized particles and is presented as:

$$\mathbf{F}_{ij}^{m} = \begin{cases} c_m \cdot \mathbf{F}_{ij}^{dipole}, & \text{for} \quad d_{ij} \le r_{ij} \le 1.5d_{ij} \\ \mathbf{F}_{ij}^{dipole}, & \text{for} \quad r_{ij} > 1.5d_{ij} \end{cases} \tag{9}$$

$$c_m = 1 + \left(3 - \frac{2r_{ij}}{d_{ij}}\right)^2 \left(\frac{60.17}{1 + e^{(\theta - 34.55)/12.52}} - 22.79\right)\frac{1}{100}$$

$$\mathbf{F}_{ij}^{dipole} = -\frac{3\mu_0}{4\pi r_{ij}^4 \mu_1}[(\mathbf{m}_i \cdot \mathbf{m}_j)\hat{\mathbf{r}} - 5(\mathbf{m}_i \cdot \hat{\mathbf{r}})(\mathbf{m}_j \cdot \hat{\mathbf{r}})\hat{\mathbf{r}} + (\mathbf{m}_j \cdot \hat{\mathbf{r}})\mathbf{m}_i + (\mathbf{m}_i \cdot \hat{\mathbf{r}})\mathbf{m}_j] \tag{10}$$

c_m is the correction factor for adjusting the magnetic dipole model to two close magnetized particles. d_{ij} is the average value of the diameters of two considered particles. Θ is the angle between the direction of the external magnetic field and the relative positional vector $\hat{\mathbf{r}} = \mathbf{r}_{ij}/r_{ij}$ and $\mathbf{F}_{ij}^{dipole}$ denotes the magnetic interaction force between two magnetic dipoles [44]. μ_0 and μ_1 are the permeability of vacuum and the matrix, respectively. $\mathbf{m}_i$ and $\mathbf{m}_j$ are the magnetic moment of particles i and j. The other numerical constants are the fitting coefficients from the data analysis.

To avoid the overlap of magnetized particles, the excluded volume force $\mathbf{F}_{ij}^{ev}$ was introduced. This force was calculated by Melle et al. as [45]:

$$\mathbf{F}_{ij}^{ev} = A\frac{3\mu_0 \mathbf{m}_i \cdot \mathbf{m}_j}{4\pi d_{ij}^4}\exp[-\xi(r_{ij}/d_{ij} - 1)]\cdot\hat{\mathbf{r}}_{ij} \tag{11}$$

where A=2 and ξ =10. The parameter A was chosen in order to give zero interaction force when two particles which align along the field direction and interact with the dipolar force are in contact.

The van der Waals force $\mathbf{F}_{ij}^{vdw}$ was also taken into account for modelling the particle–particle interaction. This force can be expressed as:[46]

$$\mathbf{F}_{ij}^{vdw} = \begin{cases} \frac{A}{24}\frac{d_{ij}}{(r_{ij} - d_{ij})^2}\hat{\mathbf{r}}, & \text{for} \quad r_{ij} - d_{ij} > h_{\min} \\ \frac{A}{24}\frac{d_{ij}}{h_{\min}{}^2}\hat{\mathbf{r}}, & \text{for} \quad r_{ij} - d_{ij} \le h_{\min} \end{cases} \tag{12}$$

where $A=5\times10^{-19}$ is the Hamaker coefficient, and $h_{min}=0.001d_{ij}$ was used. Herein, the main particle–particle interaction force model has been established.

When a particle moves in the water, it will be hindered by the viscous drag force $\mathbf{F}_i^d$ from the surrounding water. The drag force can be deduced in vector form as:

$$\mathbf{F}_i^d = -3\pi d_i \eta \mathbf{v} \tag{13}$$

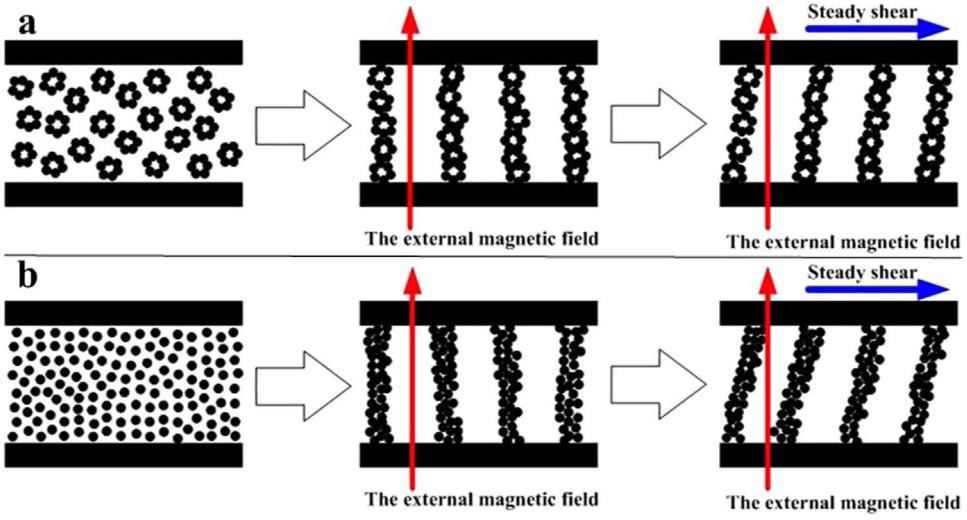

Fig. 10. Schematic of forming chain-like structure when an external magnetic field and shear were applied for the Fe_3O_4 hollow nanospheres (a) and Fe_3O_4 nanoparticles after ball-milling (b).

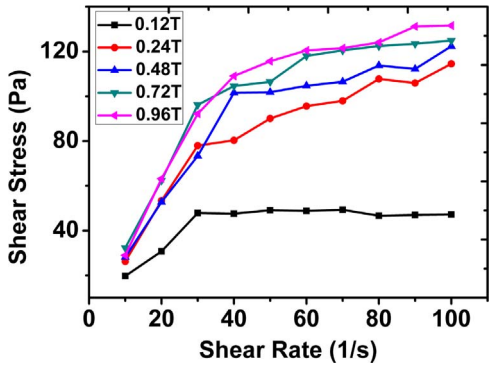

Fig. 11. The curves for shear stress versus shear rate obtained by molecular dynamic simulation under different magnetic flux density.

where **v** is the moving velocity of the particles.

The force of gravity and buoyancy applied on the particle is:

$$\mathbf{F}_i^{gb} = \frac{\pi d_i^3}{6}(\rho - \rho_w)\mathbf{g} \tag{14}$$

where ρ_w is the density of the water, ρ is the density of the particle and **g** is the gravitational acceleration.

As Fe_3O_4 hollow nanospheres are superparamagnetic material, the magnetic torque applied on the particles is so small that the magneto induced body rotational motion of the iron particles can be neglected. The inertia effect and stochastic motion of the particles were also not taken into account. This processing is reasonable because the magnetic interaction of the particles dominates their random thermal motion when an external magnetic field is applied rapidly, as discussed analogously for magnetorheological fluids by Mohebi et al. [47] With the aforementioned forces, the kinematic equation can be constructed as:

$$\begin{cases} \frac{d\mathbf{r}_i}{dt} = \frac{1}{\zeta_t}\left[\sum_{j\neq i}(\mathbf{F}_{ij}^m + \mathbf{F}_{ij}^{ev} + \mathbf{F}_{ij}^{vdw}) + \mathbf{F}_i^{gb}\right] & \text{for} \quad |\sum \mathbf{F}_i| > F_i^d \\ \frac{d\mathbf{r}_i}{dt} = 0 & \text{for} \quad |\sum \mathbf{F}_i| \le F_i^d \end{cases} \tag{15}$$

where $\zeta_t = 3\pi d_i \eta$ is the translational drag coefficient and $\sum \mathbf{F}_i$ denotes the total forces excluding the viscous drag force from the water applied on particle i. Eq. (15) can be solved using a numerical method.

A cubic cell in the magnetic fluid with an edge length of L=4 μm (about $13\times d_{50}$) was considered and periodic boundary conditions were used. The time step was 10^{-7} s and the computational steps were 3×10^6. It was assumed that the particle size distribution was uniform and the diameter of the particles was 300 nm. The weight fraction of the magnetic fluid used in this simulation was 10% and the particles dispersed in the magnetic fluid were Fe_3O_4 hollow nanospheres, the carrier liquid was redistilled water. The magnetic flux densities used in this simulation were 0.12 T, 0.24 T, 0.48 T, 0.72 T, 0.96 T, respectively. The configurations of the magneto-induced, rearrangeable microstructure in the magnetic field in a steady, uniform magnetic field would be presented.

The curves for shear stress versus shear rate were obtained by the molecular dynamic simulation (Fig. 11). Clearly, the shear stress increased rapidly with the increasing of the shear rate and then kept almost constantly which is because of the yield of the magnetic fluids. If the magnetic flux density was small, it also could be seen that the shear stress increased rapidly with the increasing of the magnetic flux density. When the magnetic flux density is large, the shear stress increased gently with the increasing of the magnetic flux density which was because of the magnetized saturation of the Fe_3O_4 hollow nanospheres.

The structure evolution which was induced by the magnetic field

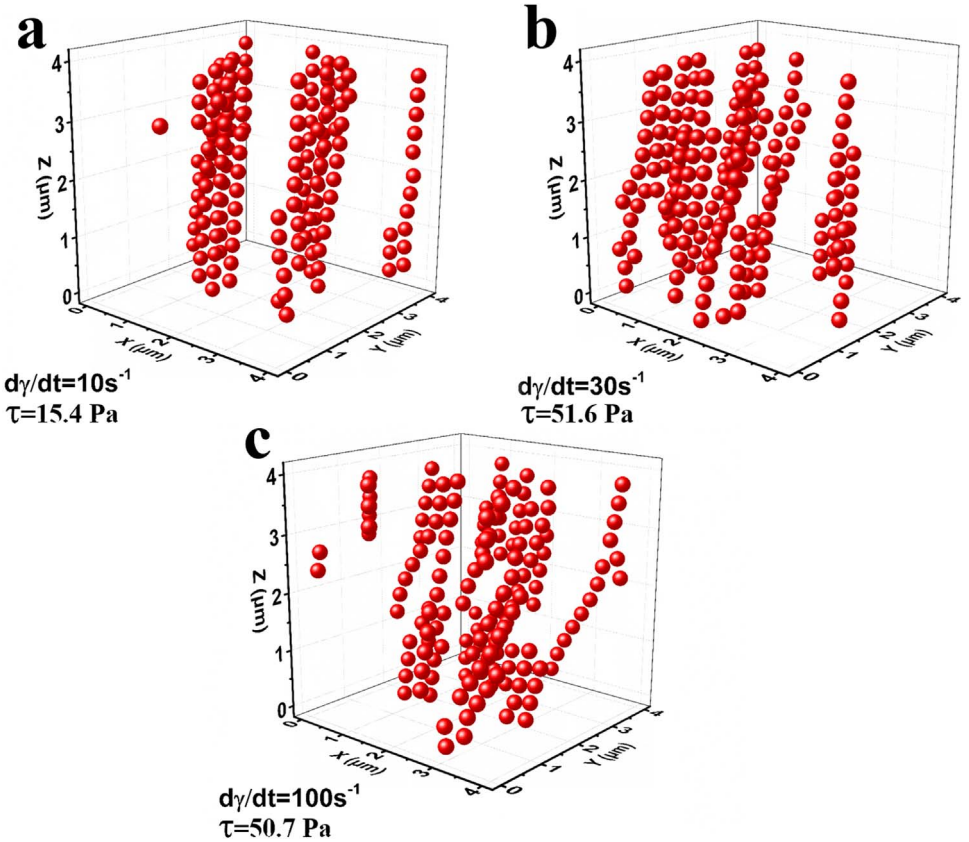

Fig. 12. The structure evolution simulation of the magnetic fluids 10 wt% based on the Fe_3O_4 hollow nanospheres and the magnetic flux density is 0.12 T; (a) for shear rate 10 (1/s), (b) for shear rate 30 (1/s), (c) for shear rate 100 (1/s).

was shown in Fig. 12. When magnetic field was imposed, the Fe_3O_4 hollow nanospheres would rapidly arrange into chains. The chains would be tilted as soon as the shear was applied. When the shear rate was small (Fig. 12a), the chains were just tilted slight and the chains were consecutive. The interaction force between the particles was strong at this time. So, the shear stress increased when the magnetic fluid suffered a shear. Along with the increasing of the shear rate, an obvious tilt of the chains appeared (Fig. 12b). Along with the sequentially increasing of the shear rate, the breakage and rebuild of the chains happened (Fig. 12c). The breakage and rebuild of the chains would reach a balance state quickly. So, the shear stress kept almost constant when the shear rate was large than 30 (1/s). The molecular dynamic simulation for the structure evolution could help us understanding the changing inside the magnetic fluid more detailed when it was suffered shear and magnetic field. The simulative results could also help us researching the properties of the magnetic fluid which were difficult to obtain with experiment more detailed.

4. Conclusions

In this work, a novel kind of Fe_3O_4 hollow nanospheres based magnetic fluid was reported and its rheological properties were analyzed. The testing results indicated the magnetic fluids presented the typical magnetorheological effect and the shear rate dependent shear stress behavior fit a typical Bingham Model. Due to the high saturation magnetization intensity of Fe_3O_4 hollow nanospheres, the shear stress of the magnetic fluid thereof could reach a maximum value about 330 Pa. Both the content of Fe_3O_4 hollow nanoparticles and the plate gap of the rheometer influenced the rheological properties. In comparison to the Fe_3O_4 nanoparticles, the Fe_3O_4 hollow nanospheres based magnetic fluid presented a better MR effect. An experiment about the stability was taken out which proved that the magnetic fluid based on Fe_3O_4 hollow nanospheres was more stable than the magnetic fluid based on Fe_3O_4 nanoparticles. A possible mechanism was proposed and it was found that the stronger chain structure was the origination. Molecular dynamic simulations about the shear stress and the structure evolution of the magnetic fluid based on Fe_3O_4 hollow nanospheres were taken out. The simulative results matched well with the experimental results and this would help us understanding the properties of the magnetic fluid more detailed. Finally, this work supplied value information for analyzing the MR mechanism and the Fe_3O_4 hollow nanospheres would have wide application in industry area.

Acknowledgements

This work was supported by Collaborative Innovation Center of Suzhou Nano Science and Technology. Financial supports from the National Natural Science Foundation of China (Grant No's. 11572309, 11572310), Anhui Provincial Natural Science Foundation of China (1408085QA17) and the National Basic Research Program of China (973 Program, Grant No. 2012CB937500) are gratefully acknowledged.

References

[1] B.J. Park, F.F. Fang, H.J. Choi, Magnetorheology: materials and application, Soft Matter 6 (2010) 5246.
[2] J. Patel, K. Parekh, R.V. Upadhyay, Maneuvering thermal conductivity of magnetic nanofluids by tunable magnetic fields, J. Appl. Phys. 117 (2015) 243906.
[3] J. Yang, S. Sun, W.H. Li, H. Du, G. Alici, M. Nakano, Development of a linear damper working with magnetorheological shear thickening fluids, J. Intell. Mater. Syst. Struct. 26 (2015) 1811–1817.
[4] I. Arief, P.K. Mukhopadhyay, Dynamic and rate-dependent yielding behavior of $Co_{0.9}Ni_{0.1}$ microcluster based magnetorheological fluids, J. Magn. Magn. Mater. 397 (2016) 57–63.
[5] V. Dixit, C.N. Nandadasa, S.G. Kim, S. Kim, J. Park, Y.-K. Hong, Site preference and magnetic properties of Ga/In-substituted strontium hexaferrite: an ab initio study, J. Appl. Phys. 118 (2015) 203908.
[6] J.R. Morillas, A.J.F. Bombard, J. de Vicente, Preparation and characterization of magnetorheological fluids by dispersion of carbonyl iron microparticles in PAO/1-octanol, Smart Mater. Struct. 25 (2016) 015023.
[7] Y. Xia, P. Yang, Y. Sun, Y. Wu, B. Mayers, B. Gates, Y. Yin, F. Kim, H. Yan, One-dimensional nanostructures: synthesis, characterization, and applications, Adv. Mater. 15 (2003) 353–389.
[8] Y. Xia, B. Gates, Y. Yin, Y. Lu, Monodispersed colloidal spheres: old materials with new applications, Adv. Mater. 12 (2000) 693–713.
[9] S. Sun, H. Zeng, Size-controlled synthesis of magnetite nanoparticles, J. Am. Chem. Soc. 124 (2002) 8204–8205.
[10] S. Sun, H. Zeng, D.B. Robinson, S. Raoux, P.M. Rice, S.X. Wang, G. Li, Monodisperse MFe_2O_4 (M=Fe, Co, Mn) nanoparticles, J. Am. Chem. Soc. 126 (2004) 273–279.
[11] J. Ge, Y. Hu, M. Biasini, C. Dong, J. Guo, W.P. Beyermann, Y. Yin, One-step synthesis of highly water-soluble magnetite colloidal nanocrystals, Chemistry 13 (2007) 7153–7161.
[12] Z. Li, L. Wei, M.Y. Gao, H. Lei, One-pot reaction to synthesize biocompatible magnetite nanoparticles, Adv. Mater. 17 (2005) 1001–1005.
[13] S. Mathur, S. Barth, U. Werner, F. Hernandez-Ramirez, A. Romano-Rodriguez, Chemical vapor growth of one-dimensional magnetite nanostructures, Adv. Mater. 20 (2008) 1550–1554.
[14] S. Lian, E. Wang, L. Gao, Z. Kang, D. Wu, Y. Lan, L. Xu, Growth of single-crystal magnetite nanowires from Fe_3O_4 nanoparticles in a surfactant-free hydrothermal process, Solid State Commun. 132 (2004) 375–378.
[15] M. Wang, W.L. Li, Y. Feng, Y.F. Hou, T.D. Zhang, W.D. Fei, J.H. Yin, Effect of BaTiO3 nanowires on dielectric properties and energy storage density of polyimide composite films, Ceram. Int. 41 (2015) 13582–13588.
[16] H. Jin Fan, M. Knez, R. Scholz, K. Nielsch, E. Pippel, D. Hesse, M. Zacharias, U. Gosele, Monocrystalline spinel nanotube fabrication based on the Kirkendall effect, Nat. Mater. 5 (2006) 627–631.
[17] S. Chen, J. Feng, X. Guo, J. Hong, W. Ding, One-step wet chemistry for preparation of magnetite nanorods, Mater. Lett. 59 (2005) 985–988.
[18] P. Aprelev, Y. Gu, R. Burtovyy, I. Luzinov, K.G. Kornev, Synthesis and characterization of nanorods for magnetic rotational spectroscopy, J. Appl. Phys. 118 (2015) 074901.
[19] C.J. Jia, L.D. Sun, Z.G. Yan, Y.C. Pang, L.P. You, C.H. Yan, Iron oxide tube-in-tube nanostructures, J. Phys. Chem. C 111 (2007) 13022–13027.
[20] K. Zhang, H.J. Choi, Fabrication and viscoelastic characteristics of amino-functionalized multi-walled carbon nanotube/poly(methyl methacrylate) nanocomposites, Compos. Struct. 125 (2015) 170–175.
[21] Y. Chen, J. Li, T. Mei, Xg Hu, D. Liu, J. Wang, M. Hao, J. Li, J. Wang, X. Wang, Low-temperature and one-pot synthesis of sulfurized graphene nanosheets via in situ doping and their superior electrocatalytic activity for oxygen reduction reaction, J. Mater. Chem. A 2 (2014) 20714–20722.
[22] D. Zhang, X. Zhang, X. Ni, J. Song, H. Zheng, Fabrication and characterization of Fe3O4 octahedrons via an EDTA-assisted route, Cryst. Growth Des. 7 (2007) 2117–2119.
[23] Q. Hua, W. Huang, Chemical etching induced shape change of magnetite microcrystals, J. Mater. Chem. 18 (2008) 4286.
[24] M.E.F. Brollo, J.M. Orozco-Henao, R. López-Ruiz, D. Muraca, C.S.B. Dias, K.R. Pirota, M. Knobel, Magnetic hyperthermia in brick-like $Ag@Fe_3O_4$ core–shell nanoparticles, J. Magn. Magn. Mater. 397 (2016) 20–27.
[25] R. Gu, X. Gong, W. Jiang, L. Hao, S. Xuan, Z. Zhang, Synthesis and rheological investigation of a magnetic fluid using olivary silica-coated iron particles as a precursor, J. Magn. Magn. Mater. 320 (2008) 2788–2791.
[26] A.A. Dubrovskiy, D.A. Balaev, K.A. Shaykhutdinov, O.A. Bayukov, O.N. Pletnev, S.S. Yakushkin, G.A. Bukhtiyarova, O.N. Martyanov, Size effects in the magnetic properties of ε-Fe_2O_3 nanoparticles, J. Appl. Phys. 118 (2015) 213901.
[27] X. Liu, D. Ye, X. Gao, F. Li, M. Sun, H. Zhang, T. Tu, H. Yu, Normal force for static and steady shear mode in magnetorheological fluid, J. Magn. Magn. Mater. 398 (2016) 137–140.
[28] Y.J. Kim, Y.D. Liu, Y. Seo, H.J. Choi, Pickering-emulsion-polymerized polystyrene/Fe_2O_3 composite particles and their magnetoresponsive characteristics, Langmuir 29 (2013) 4959–4965.
[29] J.R. Morillas, E. Carreon-Gonzalez, J. de Vicente, Effect of particle aspect ratio in magnetorheology, Smart Mater. Struct. 24 (2015).
[30] L. Rodriguez-Arco, M.T. Lopez-Lopez, A.Y. Zubarev, K. Gdula, J.D. Duran, Inverse magnetorheological fluids, Soft Matter 10 (2014) 6256–6265.
[31] Z. Liu, X. Zhou, Y. Zhang, Q. Liu, Q. Liu, B. Li, G. Zhu, D. Li, X. Li, Fabrication of monodispersed, uniform rod-shaped $FeCO_3/CoCO_3$ microparticles using a facile solvothermal method and their excellent microwave absorbing properties, J. Alloy. Compd. 665 (2016) 388–393.
[32] M. Krajewski, K. Brzozka, W.S. Lin, H.M. Lin, M. Tokarczyk, J. Borysiuk, G. Kowalski, D. Wasik, High temperature oxidation of iron-iron oxide core-shell nanowires composed of iron nanoparticles, Phys. Chem. Chem. Phys. 18 (2016) 3900–3909.
[33] P. Zhang, K.H. Lee, C.H. Lee, Friction behavior of magnetorheological fluids with different material types and magnetic field strength, Chin. J. Mech. Eng. 29 (2015) 84–90.
[34] Q. Zhang, I. Lee, J.B. Joo, F. Zaera, Y. Yin, Core–shell nanostructured catalysts, Acc. Chem. Res. 46 (2012) 1816–1824.
[35] K. Zhang, S. Piao, H. Choi, Hollow structured magnetic particles of $CoFe_2O_4$ and their magnetorheological characteristics, IEEE Trans. Magn. 51 (2015) 1–4.
[36] Z. Cao, W. Jiang, X. Ye, X. Gong, Preparation of superparamagnetic Fe3O4/PMMA nano composites and their magnetorheological characteristics, J. Magn. Magn. Mater. 320 (2008) 1499–1502.
[37] S. Xuan, L. Hao, K.C.-F. Leung, Shear disassembly of hierarchical superparamag-

netic Fe3O4hollow nanoparticle necklace chains, New J. Chem. 38 (2014) 6125–6132.
[38] L. Rodríguez-Arco, M.T. López-López, P. Kuzhir, J.D.G. Durán, Steady state rheological behaviour of multi-component magnetic suspensions, Soft Matter 9 (2013) 5726.
[39] B. Sim, H.S. Chae, H.J. Choi, Fabrication of polyaniline coated iron oxide hybrid particles and their dual stimuli-response under electric and magnetic fields, Express Polym. Lett. 9 (2015) 736–743.
[40] D.J. Klingenberg, F. van Swol, C.F. Zukoski, The small shear rate response of electrorheological suspensions. II. Extension beyond the point–dipole limit, J. Chem. Phys. 94 (1991) 6170.
[41] C. Guo, X. Gong, S. Xuan, Q. Yan, X. Ruan, Squeeze behavior of magnetorheological fluids under constant volume and uniform magnetic field, Smart Mater. Struct. 22 (2013) 045020.
[42] X.L. Gong, F. Yang, S.H. Xuan, L.H. Zong, W. Zhu, W.Q. Jiang, Boundary effect in electrorheological fluids, Phys. Rev. E 84 (2011).
[43] T. Liu, X. Gong, Y. Xu, S. Xuan, W. Jiang, Simulation of magneto-induced rearrangeable microstructures of magnetorheological plastomers, Soft Matter 9 (2013) 10069.
[44] J.P. Segovia-Gutiérrez, J. de Vicente, R. Hidalgo-Álvarez, A.M. Puertas, Brownian dynamics simulations in magnetorheology and comparison with experiments, Soft Matter 9 (2013) 6970.
[45] S. Melle, O.G. Calderón, M.A. Rubio, G.G. Fuller, Rotational dynamics in dipolar colloidal suspensions: video microscopy experiments and simulations results, J. Non-Newton. Fluid Mech. 102 (2002) 135–148.
[46] D. Klingenberg, C. Olk, M. Golden, J. Ulicny, Effects of nonmagnetic interparticle forces on magnetorheological fluids, J. Phys.: Condens. Matter 22 (2010) 324101.
[47] M. Mohebi, N. Jamasbi, J. Liu, Simulation of the formation of nonequilibrium structures in magnetorheological fluids subject to an external magnetic field, Phys. Rev. E 54 (1996) 5407.